Ethanol sensitivity of thermally evaporated nanostructured WO_3 thin films doped and implanted with Fe

M. Ahsan, M.Z.Ahmad*, T. Tesfamichael, J. Bell and Prasad KDV Yarlagadda

Chemistry, Physics and Mechanical Engineering School, Science and Engineering Faculty, Queensland University of Technology, Brisbane, Australia.

*Department of Mechanical Engineering, RMIT University, Melbourne, Australia
Contact E-Mail: y.prasad@qut.edu.au

Keywords: Gas Sensors, Ethanol, Nano-Structured Materials, Thin Films

Abstract: Ethanol sensing performance of gas sensors made of Fe doped and Fe implanted nanostructured WO_3 thin films prepared by a thermal evaporation technique was investigated. Three different types of nanostructured thin films, namely, pure WO_3 thin films, iron-doped WO_3 thin films by co-evaporation and Fe-implanted WO_3 thin films have been synthesized. All the thin films have a film thickness of 300 nm. The physical, chemical and electronic properties of these films have been optimized by annealing heat treatment at 300ºC and 400ºC for 2 hours in air. Various analytical techniques were employed to characterize these films. Atomic Force Microscopy and Transmission Electron Microscopy revealed a very small grain size of the order 5-10 nm in as-deposited WO_3 films, and annealing at 300ºC or 400ºC did not result in any significant change in grain size. This study has demonstrated enhanced sensing properties of WO_3 thin film sensors towards ethanol at lower operating temperature, which was achieved by optimizing the physical, chemical and electronic properties of the WO_3 film through Fe doping and annealing.

Introduction

Of the different gas sensors, semiconductor based chemiresistor sensors are most investigated and widely used for detection of combustible and toxic gases owing to their low cost and relative simplicity. The Chemiresistive gas sensor works on the principle of a change in electrical resistance due to an interaction between the semiconductor and the gas. Various semiconducting oxides, catalytic oxides and mixed oxides [1-10] have been investigated for gas sensing properties and many more oxides are now currently being explored. The gas sensing properties of these oxides are determined by their intrinsic properties, however, can be modified by addition of impurities and modifying the microstructure including particle size, orientation and distribution, surface morphology and porosity [11]. The operating temperature strongly influences the sensitivity of the sensor [12] since the reactions occurring at the surface of the sensor (chemisorption/redox reaction) are functions of temperature. Use of additives such as Pd, Pt, In, Cu, Nb, Mn, Si to improve the sensor response has been extensively reported in the literature [13-15]. Tungsten trioxide (WO_3) is a well-known n-type semiconductor with a band gap of 2.6 eV that has been used not only in catalytic/photocatalytic [16], electrochromic applications [17] but also in solid state gas sensors. It has been successfully used to detect NH_3, H_2S, NO_2, O_3, H_2 and VOC. However, it is less sensitive to carbon monoxide and hydrocarbons [18]. Iron addition lower than 10 at% to WO_3 films prepared by reactive RF sputtering produced an enhancement in sensor response when exposed to NO_2 [19]. Iron addition was found to be advantageous in sensing ozone, CO and ethanol. NO_2 and humidity sensing characteristics of WO_3 thin films prepared by vacuum thermal deposition and subsequent annealing in the temperature range of 300-600^{o}C were investigated by Xie et al [20]. It was found that NO_2 sensing was strongly dependant on annealing and working temperature. In the present work, WO_3thin films were deposited by thermal evaporation technique to produce nanostructured films with higher porosity that are suitable for gas sensing applications. Small amount of iron was added to WO_3 films by co- evaporation as well as implantation. The affect of physical, chemical and electronic properties on ethanol sensing performance of these films has been investigated.

Experimental

Thermal evaporation was used to deposit thin films of tungsten oxide and iron-doped tungsten oxide (0.5 at% Fe). WO_3 thin films were deposited on silicon substrates with interdigitated Pt electrodes (Electronics Design Center, Case Western Reserve University, Cleveland, USA). The size of the substrate was 8 mm x 8 mm x 0.5 mm. The electrode fingers have a line width and line thickness of 100 μm and a height of 300 nm, respectively. Tungsten oxide (99.9% purity) and iron powder (99.9% purity) of sizes 20 μm and 100 μm, respectively (Sigma Aldrich Pty Ltd) were used as evaporation sources. Before the deposition, the powders were placed in dessicator to avoid any moisture and decontamination. For the purpose of doping, iron was mixed thoroughly with WO_3 and the mixture was evaporated. A bell jar type PVD unit (Varian Coater with AVT Control System, Australia) was used to deposit the WO_3 thin films. The substrates were mounted on a substrate holder which was placed at a distance of 38 cm in line of sight from the evaporation source. Deposition was carried out at 4 x 10^{-5} mbar. Powder was deposited onto the substrates at a rate of 35 nm per second. A quartz crystal film thickness monitor was used to control the thickness of films which was restricted to 300 nm. In order to implant the WO_3 thin films with small amount of iron, the ion implantation facility at Australian Nuclear Science and Technology Organization (ANSTO) was employed. Samples of WO_3 thin film were mounted on a rotating sample holder with a good electrical contact, which reduced charging effects during ion implantation. Implantation was performed in a vacuum chamber, which was evacuated to a base pressure of about 3×10^{-6} mbar. After achieving the required vacuum, a high current was applied to the Fe cathode to generate Fe ion beam. The beam was incident normally onto the sample surface at 40 KeV. Uniformity of the implantation was assured by sweeping the sample across the ion beam. After the deposition, the films were annealed at 400^{o}C for 2 hours in air to improve the microstructural properties and relieve any thermal stresses in the films.

A JEOL 1200 TEM was used at an accelerating voltage of 120 kV to investigate the size and shape of WO_3 nanoparticles, crystalline structure and distribution of dopant in the film. An NT-MDT P47 Solver Scanning Probe Microscope was used to study the surface morphology of the films. The WO_3 film surface was scanned by a silicon tip (radius of curvature 10 nm) in semi-contact mode over an area ranging from 500 x 500 nm^2 to 2000 x 2000 nm^2. The mean grain size and grain distribution and surface roughness were determined by using the Nova NT-MDT Image Analysis Software. The concentration profile of constituent elements in WO_3 film was determined using RBS analysis. RBS measurements were carried out with a 1.8 MeV He^+ beam under a vacuum of 7 x 10^{-4} Pa. XPS analysis was performed using Kratos AXIS Ultra XPS incorporating a 165 mm hemispherical electron energy analyser, and using monochromatic Al K X-rays (1486.6 eV) at 150 W (15 kV, 10 mA), incident at 45^{o} to the sample surface. Photoelectron data was collected at take off angle of 90^{o}. Survey (wide) scans were taken at analyser pass energy of 160 eV and multiplex (narrow) high resolution scans at 20 eV. Survey scans were carried out over 1200-0 eV binding energy range with 1.0 eV steps and a dwell time of 100 ms. Narrow high-resolution scans were run with 0.05 eV steps and 250 ms dwell time. Base pressure in the analysis chamber was 1.0 x 10^{-9} torr and during sample analysis 1.0 x 10^{-8} torr. Raman measurements were performed using an Oceanoptics QE 6500 spectrometer. A 532 nm line from an argon ion laser was used as the excitation source. To avoid local heating of the samples, small power of about 5 mW was used on the samples. A raman shift between wavenumbers 200 cm^{-1} and 1200 cm^{-1} has been measured. The WO_3 sensor responses to various concentrations (10-1000 ppm) of ethanol at various operating temperatures (100^{o}C to 300^{o}C) were measured. Ethanol was diluted in synthetic air to achieve the desired concentrations. For all the experiments, the total flow was adjusted to 200 sccm. The gas sensing performance of the films to reducing gases such as ethanol denoted as $S_{reducing}$ is defined as the ratio:

$$S_{reducing} = \frac{R_{air} - R_{gas}}{R_{gas}} X\,100 \qquad (1)$$

where R_{air} is the resistance in air under stationary conditions and R_{gas} represents the resistance after the sensor is exposed to the target gas during a definite time. Equation (1) can be applied for n-type material such as WO_3 and reducing gas such as CO.

The response curve was recorded under a continuous flow of known amount of CO. A sequence control computer was utilized to computerize the pulse sequence of the CO concentrations. Initially, synthetic air was passed through the chamber at testing temperature until the stable baseline resistance was observed. Then a sequence of target gas pulse was generated for 10 minutes followed by synthetic air pulse. This procedure was continued until a stable baseline was observed after alternate pulses. This was followed by the experimental sequence of pulses and data was recorded. Each sensor was tested at temperatures between 100^{o}C to 300^{o}C at intervals of 50^{o}C under various concentrations of CO, and optimum operating temperature was determined. This was followed by two full range tests for each sensor and CO at the optimum operating temperature.

Results and Discussion

The AFM surface topography of as-deposited WO_3 film (Fig. 1a) shows a nanostructured surface with well defined grains of mean size and roughness of ~13 nm and 0.5 nm, respectively, as obtained by NT-MDT Nova Image Analysis Software. The TEM image of the film (Fig. 1b) reveals a dense structure and grain size of about 10-15 nm. The broad and hazy ring around the center spot in selected-area diffraction pattern (SADP) indicates highly amorphous nature of the WO_3 film (inset in Fig. 1b). Annealing of the as-deposited WO_3 film at 300ºC for 2 hours in air resulted in the reduction of the grain size from 13 nm to 10 nm as shown by the AFM (Fig. 2a), but no change was observed in roughness. The TEM image (Fig. 2b) shows a very compact and dense film. The halo diffraction pattern (inset in Fig. 2b) indicates that the film is still amorphous. Annealing of WO_3 films at 400ºC in air for 2 hours resulted in crystalline grain growth with well defined grains of mean size of ~ 5 nm (Fig. 3). The film appears to be loosely packed after annealing at 400ºC. The bright spots in the diffraction pattern (inset in Fig. 3) show that the film is highly crystalline.

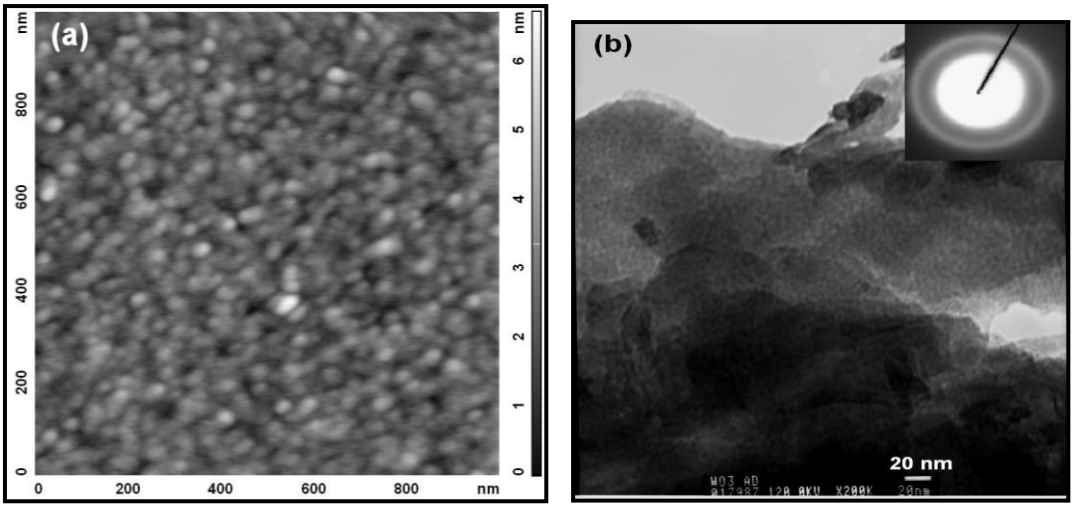

Figure 1: AFM semicontact mode image (a) and TEM image (b) of as-deposited nanostructured WO_3 film.

The AFM surface topography of as-deposited Fe-doped WO_3 film is shown in Fig. 4. The surface reveals well defined grain boundaries with an average grain size of 15 nm (Fig. 4a). However, the grains appear to be densely packed as compared to the pure WO_3 film (Fig. 1a). Addition of iron also resulted in an increase in roughness to 0.6 nm as compared to 0.5 nm for as-deposited WO_3 film. The TEM image (Fig.4b) reveals a compact structure and a mean grain size of about 15 nm, which is consistent with the AFM results. The halo pattern in the SADP indicates the amorphous nature of Fe-doped WO_3 film (inset in Fig. 4b). The surface topography of Fe-doped WO_3 film annealed at 300ºC for 2 hours in air is shown in Fig. 5. Annealing at 300ºC decreased the grain size from 15 nm to 10 nm (Fig. 5a) and surface roughness from 0.6 to 0.5 nm.

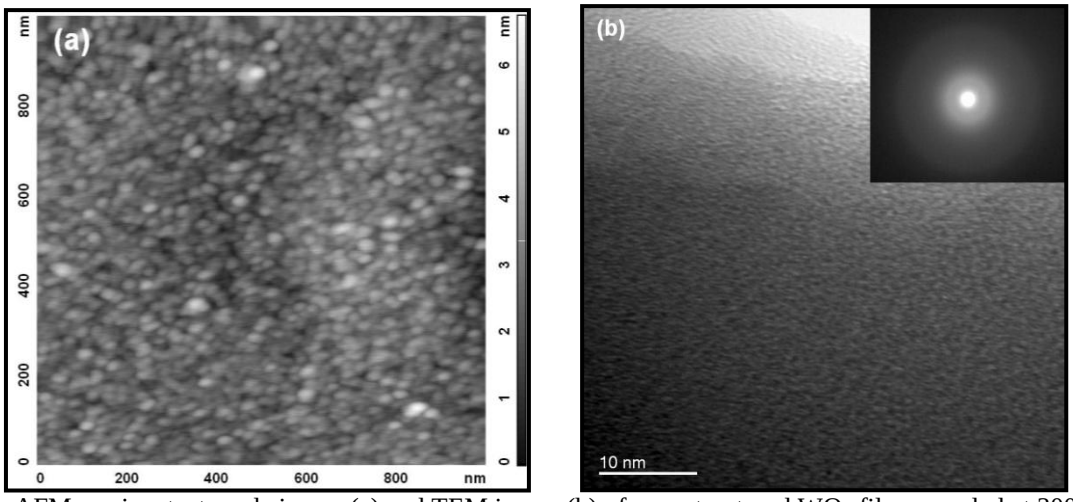

Figure 2: AFM semicontact mode image (a) and TEM image (b) of nanostructured WO_3 film annealed at 300ºC for 2 hours in air.

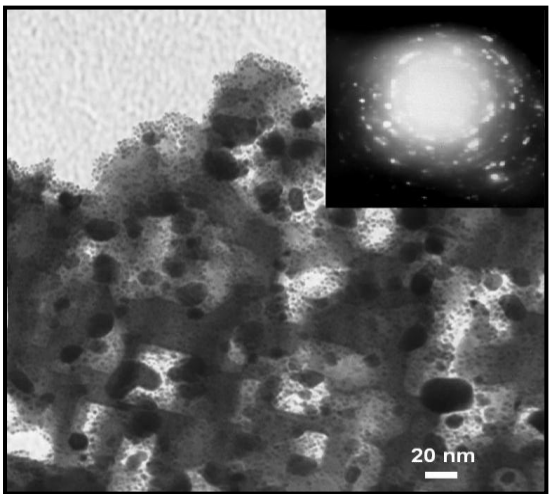

Figure 3: TEM image of nanostructured WO_3 film annealed at 400ºC for 2 hours in air.

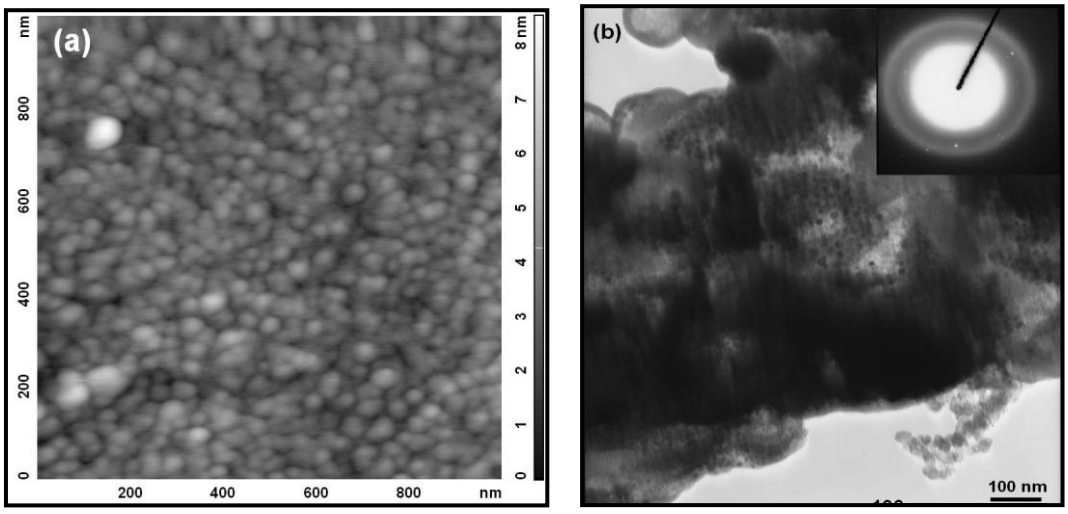

Figure 4: AFM semicontact mode image (a) and TEM image (b) of as-deposited nanostructured Fe-doped WO_3 film.

Doping with iron and subsequent annealing at 300ºC results in a topography whcih is similar to the pure WO_3 film annealed at 300ºC (Fig. 2a). The TEM image of this film (Fig. 5b) shows a densely packed structure. The film appears to be significantly amorphous, as it is evidenct from dominant continuous rings (inset in Fig. 5b).

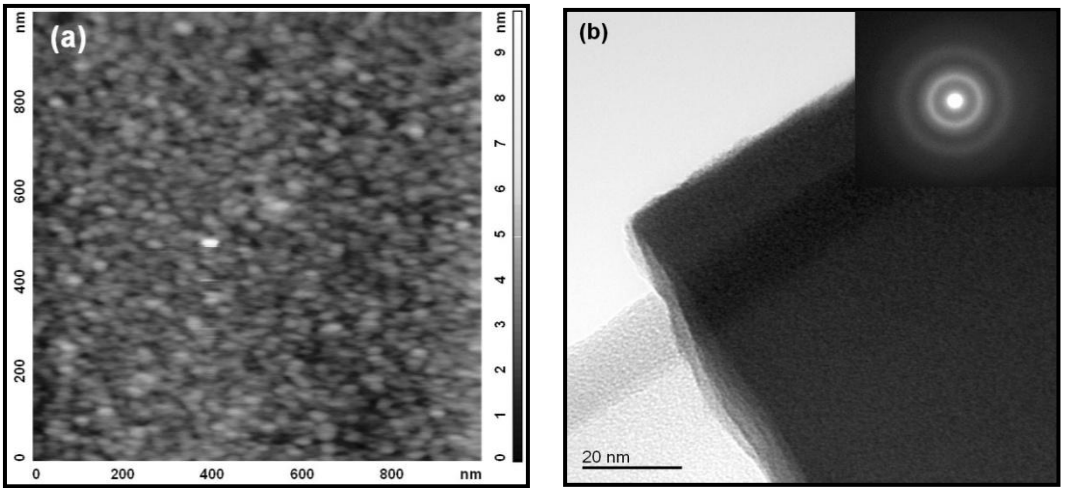

Figure 5: AFM semicontact mode image (a) and TEM image (b) of nanostructured Fe-doped WO_3 film annealed at 300ºC for 2 hours in air.

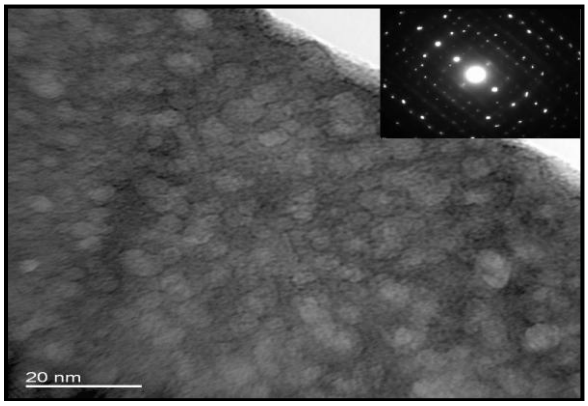

Figure 6: TEM image of nanostructured Fe-doped WO_3 film annealed at 400ºC for 2 hours in air.

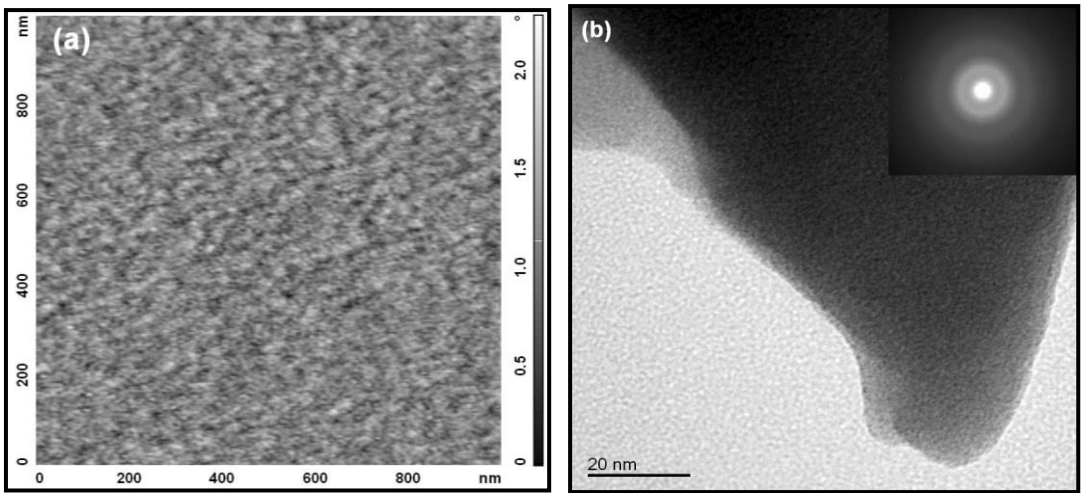

Figure 7: AFM semicontact mode image (a) and TEM image (b) of nanostructured Fe-implanted WO_3 film.

Fig. 6 shows the TEM image of Fe-doped WO_3 film annealed at 400ºC for 2 hours in air. A mean grain size of the order of 5-10 nm is observed. Annealing at 400ºC induced significant crystallinity in the film, indicated by bright spots in the diffraction pattern (inset in Fig. 6). The film appears to have less dense structure upon annealing at 400ºC, which was not observed in as-deposited or 300ºC annealed Fe-doped WO_3 films. The crystallinity of this film is similar to that of 400ºC annealed WO_3 film but with a slightly larger grain size. The surface topography of Fe-implanted WO_3 film shows a nanostructured surface with a grain size of less than 10 nm and a mean roughness of 0.2 nm (Fig. 7a). The image was obtained in phase contrast mode as the semicontact

topography mode was unable to resolve the surface. The film shows a densely packed surface and a very small grain size. The TEM image (Fig. 7b) also shows a very dense and compact film characterized by a highly amorphous nature, as observed by the diffraction pattern (inset in Fig. 7b).

Upon annealing the Fe-implanted WO_3 film at 300ºC for 2 hours in air, a slight improvement in surface topography, characterized by small clusters consisting of few grains (Fig. 8) is observed. The grain size is less than 10 nm and roughness is reduced to 0.1 nm. The TEM image (Fig. 8b) shows a dense and compact film with a highly damaged surface. The film appears to be predominantly amorphous, as observed from the diffraction pattern (inset in Fig. 8b). Fig. 9 shows the TEM image of Fe-implanted WO_3 film annealed at 400ºC for 2 hours in air. The film appears to be very dense and highly amorphous as indicated by the inset in Fig. 9. The grain size could not be quantified from TEM analysis in this case.

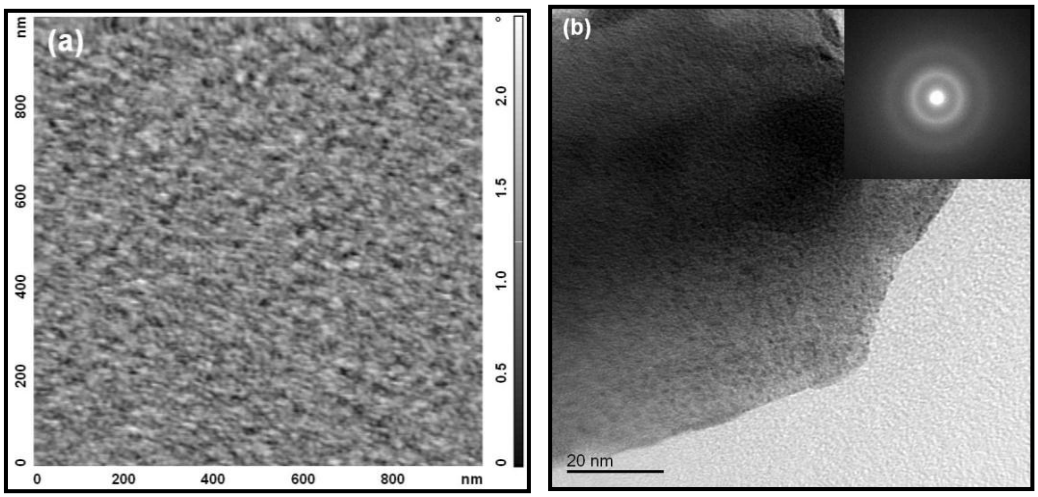

Figure 8: AFM semicontact mode image (a) and TEM image (b) of nanostructured Fe-implanted WO_3 film annealed at 300ºC for 2 hours in air.

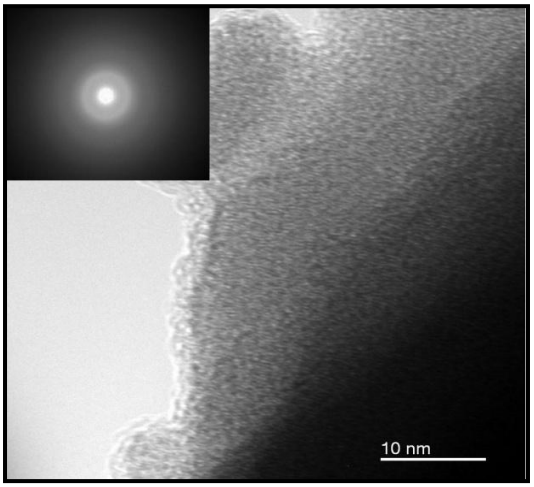

Figure 9: TEM image of nanostructured Fe-implanted WO_3 film annealed at 400ºC for 2 hours in air.

Conclusions

Highly amorphous nanostructured WO_3, Fe-doped WO_3 and Fe-implanted WO_3 thin films (300 nm thick) with a grain size less than 15 nm have been synthesized using thermal evaporation technique. The as-deposited WO_3 films showed a highly unstable response ethanol, owing to their amorphous nature. Doping with small amount (0.5 at.%) of iron considerably improved the sensing performance. Upon implantation with 5.5 at.% of Fe, the film became highly amorphous. Annealing at 300ºC for 2 hours in air showed an onset of the crystalline properties of pure and Fe-doped WO_3

films and induced sub-stoichiometry in these films. These films showed a response towards ethanol, the response was characterized by noise and a drifting baseline. Annealing at 400ºC for 2 hours significantly improved the crystalline properties and altered the stoichiometry in the WO_3 and Fe-doped WO_3 films, which increased the number of oxygen vacancies in the films. An increase in number of oxygen vacancies is considered to be highly beneficial for gas sensing. A response to ethanol was observed at an optimum operating temperature of 150ºC. The Fe-implanted WO_3 film annealed at 400ºC did not show any response to ethanol in the temperature range 100ºC-300ºC.

References

1. Korotcenkov, G., et al., Thin Solid Films, 2004. **460**(1-2): p. 315-323.
2. Liu, Z., et al., T*hin films.* Sensors and Actuators B: Chemical, 2007. **128**(1): p. 173-178.
3. Mutschall, D., K. Holzner, and E. Obermeier, Sensors and Actuators B: Chemical, 1996. **36**(1-3): p. 320-324.
4. Ryzhikov, A., M. Labeau, and A. Gaskov, Sensors and Actuators B: Chemical, 2005. **109**(1): p. 91-96.
5. Seiyama, T., *Chemical Sensor Technology*. Vol. 1. 1988, Tokyo: Kodansha Ltd./Elsevier.
6. Solis, J.L., et al., Thin Solid Films, 2001. **391**(2): p. 255-260.
7. Verma, M.K. and V. Gupta, Sensors and Actuators B: Chemical. **166-167**(0): p. 378-385.
8. Wu, R.J., et al., Sensors and Actuators B: Chemical, 2009. **138**(1): p. 35-41.
9. Yamazoe, N., G. Sakai, and K. Shimanoe, Catalysis Surveys from Asia, 2003. **7**(1): p. 63-75.
10. Zheng, L., M. Xu, and T. Xu, Sensors and Actuators B: Chemical, 2000. **66**(1-3): p. 28-30.
11. Jiménez, I., et al., Sensors and Actuators B: Chemical, 2003. **93**(1-3): p. 475-485.
12. Ihokura, H., *SnO_2 based inflammable gas sensors*. 1983, Kyushu University: Japan. p. 52-57.
13. Galatsis, K., et al., Sensors and Actuators B, 2003. **93**: p. 562-565.
14. Rani, S., S.C. Roy, and M.C. Bhatnagar, Sensors and Actuators B: Chemical, 2007. **122**(1): p. 204-210.
15. Ruiz, A.M., et al., Sensors and Actuators B: Chemical, 2005. **108**(1-2): p. 34-40.
16. Lietti, L., et al., Catalysis Today, 1996. **29**(1-4): p. 143-148.
17. Granqvist, C.G., *Handbook of Inorganic Electronic Materials*. 1995, Amsterdam: Elsevier.
18. Wang, H.T., et al., Applied Physics Letters, 2005. **86**(24): p. 243503-243503-3.
19. Comini, E., et al., Sensors and Actuators B: Chemical, 2007. **127**(1): p. 22-28.
20. Xie, G., et al., Sensors and Actuators B: Chemical, 2007. **123**(2): p. 909-914.
21. Cantalini, C., et al., Sensors and Actuators B: Chemical, 1996. **35**(1-3): p. 112-118.
22. Choi, Y.-G., et al., Sensors and Actuators B: Chemical, 2003. **95**(1-3): p. 258-265.
23. Hoel, A., et al., Current Applied Physics, 2004. **4**(5): p. 547-553.
24. Siciliano, T., et al., Sensors and Actuators B: Chemical, 2008. **133**(1): p. 321-326.
25. Song, S.-K., et al., Sensors and Actuators B: Chemical, 1998. **46**(1): p. 42-49.
26. Lethy, K.J., et al., Applied surface Science, 2008. **254**: p. 2369-2376.
27. Salje, E. and K. Viswanathan, Acta Crystallographica A, 1975. **31**(3): p. 356-359.
28. Guery, C., et al., Journal of Solid State Electrochemistry, 1997. **1**(3): p. 199-207.
29. Morar, J.F., et al., J. of Vacuum Science and Tech. A: Vacuum, Surfaces and Films, 1985. **3**(3): p. 1477-1480.
30. Yao, J.N., P. Chen, and A. Fujishima, Journal of Electroanalytical Chemistry, 1996. **406**(1-2): p. 223-226.
31. Maffeis, T.G.G., et al., e-Journal of Surface Science and Nanotechnology, 2009. **7**: p. 319-322.
32. Regragui, M., et al., Thin Solid Films, 2000. **358**(1-2): p. 40-45.
33. Hollinger, G. 1976, Thesis, Universite Claude Bernad: Lyon.
34. Santucci, S., et al., Journal of Vacuum Science and Technology, 2000. **18**(4): p. 1077.
35. Granqvist, C.G., *CRC Handbook of Solid State Electrochemistry*, ed. P.J. Gellings and H.J.M. Bouwmesster. 1997, Cleveland and Ohio: CRC Press, Inc.
36. Yamazoe, N.,. Sensors and Actuators B: Chemical, 1991. **5**(1-4): p. 7-19.
37. Maffeis, T.G.G., et al., Surface Science, 2007. **601**(21): p. 4953-4957.
38. Khyzhun, O.Y., Journal of Alloys and Compounds, 2000. **305**(1-2): p. 1-6.
39. Sanders, B.W., J. Yao, and M.L. Post, MRS Proceedings, 1994. **343**: p. 463.
40. Gopel, W. and K.D. Schierbaum,. Sensors and Actuators B, 1995. **26**(27): p. 1.
41. Yamazoe, N., et al.,. Surface Science, 1979. **86**: p. 335-344.